energies

MDPI

Article

Automatic Resonance Compensation for Efficient WPT via Magnetic Resonance Coupling Using Flexible Coils

Sousuke Nakamura [1,*], Katsuki Baba [2] and Takahiro Miyaura [3]

[1] Faculty of Science and Engineering, Hosei University, Tokyo 184-1584, Japan
[2] Graduate School of Science and Engineering, Hosei University, Tokyo 184-1584, Japan; katsuki.baba.5j@stu.hosei.ac.jp
[3] Charging System Division, Engineering Department, DAIHEN Corporation, Osaka 532-1852, Japan; t-miyaura@daihen.co.jp
* Correspondence: snakamura@hosei.ac.jp

Abstract: With the recent proliferation of mobile and wearable devices, wireless power transfer (WPT) has gained attention as an up-and-coming technology to charge these devices. In particular, WPT via magnetic resonance coupling has attracted considerable interest for day-to-day applications since it is harmless to the human body and has relatively long transmission distance. However, it was difficult to be installed into environment (e.g., utensils and furniture) and flexible objects in the living space since the use of flexible coils leads to the decrease in transmission efficiency due to the collapse of the resonance caused by coil deformation. Therefore, this study proposes an automatic resonance compensation system that automatically compensates the inductance variation caused by coil deformation using a circuit that can electronically control the equivalent capacitance (a capacity control circuit), and thereby maintains the resonant state. An experiment was conducted to verify whether the efficiency was maintained when the coil deformed. The results indicated a transmission efficiency nearly as high as that of the ideal resonant state as well as a highly responsive control, and therefore, the proposed system has a good potential for use in real-world applications.

Keywords: wireless power transfer (WPT); magnetic resonance coupling; flexible coil; automatic resonance compensation

Citation: Nakamura, S.; Baba, K.; Miyaura, T. Automatic Resonance Compensation for Efficient WPT via Magnetic Resonance Coupling Using Flexible Coils. *Energies* **2021**, *14*, 5254. https://doi.org/10.3390/en14175254

Academic Editor: Dong-Wook Seo

Received: 23 June 2021
Accepted: 19 August 2021
Published: 25 August 2021

1. Introduction

The proliferation of mobile and wearable devices is making its power management troublesome, and under this circumstance, wireless power transfer (WPT) has gained attention as an up-and-coming technology to charge these devices. In particular, there is a growing interest in the use of WPT by magnetic resonance coupling [1–8] in day-to-day applications because of its broader transmission range compared with electromagnetic induction [9], higher transmission efficiency and relatively low impact on the human body compared with microwaves [10] and laser [11].

However, since rigid coils were mostly used in WPT via magnetic resonance coupling, it was difficult to be installed into environment (e.g., utensils and furniture) and flexible objects in the living space. For this reason, the application of WPT has been limited so far. Here, using flexible and deformable coils instead of rigid coils will open the way to embed power transmission coils into flexible utensils and furniture (and thereby expand the WPT area), as well as flexible objects and devices (and thereby expand the WPT-compatible options). For example, it would be possible to expand the power transfer area by embedding a flexible coil into sofas, reclining chairs, and back cushions. Furthermore, soft objects and devices such as plush toys with monitoring cameras, skin patch/body wrapped biosensors and electrical muscle stimulation (EMS) devices, and haptic gloves could be turned into WPT-compatible by installing a flexible coil. These situations could be indicated graphically as Figure 1a. Looking from the other point of view, attaching flexible

coils to home appliances of different shapes and making them WPT-compatible could be another application (Figure 1b). Outside the realm of living spaces, sensors with flexible coils can be attached to the internal wall of pipes to monitor their internal condition [12–15] (Figure 1c). Therefore, the use of flexible coils will expand the applicability of WPT via magnetic resonance coupling, but so far, this was not widely available due to concerns such as reduction in transmission efficiency.

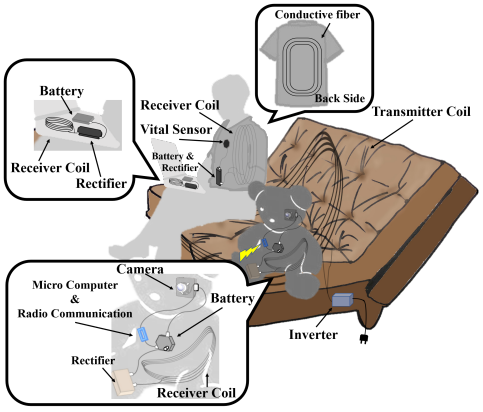

(**a**) Example of a flexible coil used in living spaces

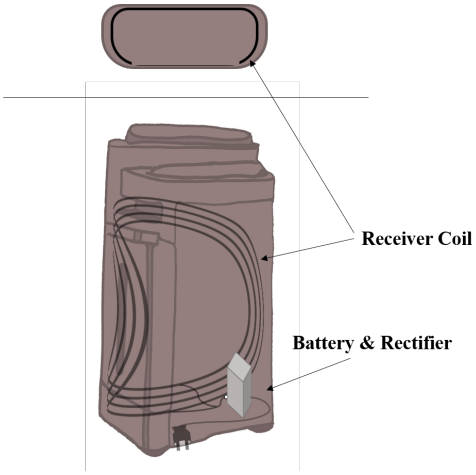

(**b**) Example of a flexible coil embedded in home appliances such as air cleaner

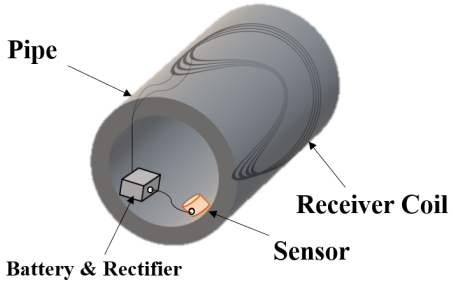

(**c**) Example of a flexible coil attached to a pipe

Figure 1. Examples of applications of WPT using flexible coils. (**a**) Used in living spaces (**b**) Embedded in home appliances (**c**) Attached to a curved shape

In WPT via magnetic resonance coupling, a condition for a high-efficiency power transfer is that the resonance frequency of the circuit and the frequency of the power source are matching. Thus, it ends up in a decrease in transmission efficiency when the flexible coil is used, since the resonance frequency of the circuit changes due to inductance variation caused by deformation of the flexible coil. Therefore, to supply power wirelessly with high efficiency using flexible coils, it is necessary to set or control the capacitance value of external capacitors to ensure resonance according to the coil shape (inductance value).

To date, there has been not so much research on WPT using flexible coils via magnetic resonance coupling compared to that via electromagnetic induction. Some studies assumed that the shape of the flexible coil does not change. For example, a study that dealt with theoretically calculating self-inductance and mutual inductance of flexible coils of free-form surface to determine the capacitance value of external capacitors was conducted [16]. In contrast, there are studies that considered the shape change of flexible coil as well. For example, one study proposed making design changes such as making the coil smaller or tightening the coil winding to reduce the drop in transmission efficiency due to resonance loss caused by coil shape change [17]. However, there is no guarantee that such design

changes can be applied to a power receiver coil, and even if it is possible, a certain efficiency drop will still occur when the shape changes.

Therefore, this study proposes a practical method that automatically controls the capacitance value of external capacitors to counter the efficiency drop caused by the shape change of flexible coils. We propose a method of resonance compensation by automatic control of the capacitance value of external capacitors according to changes in the shape of flexible coils.

The two main contributions of this paper are as follows: First, it offers an automatic resonance compensation system that maintains a high transmission efficiency despite changes in the coil shape in WPT via magnetic resonance coupling using flexible coils. Here, we proposed a simple but practical method which maximize the apparent power ratio using hill-climbing method in order to maximize the transmission efficiency. It should be noted that the capacity control circuit itself was also modified to support serial-serial WPT. Secondly, we demonstrated via actual experiments that the proposed system is able to maintain a level of transmission efficiency nearly as high as that of the ideal resonant state, while it also shows enough control responsiveness.

2. Efficiency Compensation by Capacity Control in Case of Using Flexible Coils

This section looks at how the deformation of a flexible coil used on the power receiver side affects transmission efficiency. Moreover, we verify that the maximum efficiency is achieved during resonance based on the electrical circuit theory. Finally, the effectiveness of efficiency compensation by capacity control is detailed.

Figure 2 shows the equivalent circuit of the series-series (SS) WPT via magnetic resonance coupling dealt with in this paper. Here, as the reactance of the transmitter side does not affect the transmission efficiency (in reality, there is a slight effect due to the presence of internal resistance, but it is ignored) [18], in this study, the reactance of the transmitter side is considered 0 (i.e., transmitter side is in resonant state) for the sake of simplicity and for focusing on the transmission efficiency. Equation (1) shows the formula of transmission efficiency η for this case. The changes in the circuit element values due to the coil deformation and the effect of these changes on the transmission efficiency are as follows.

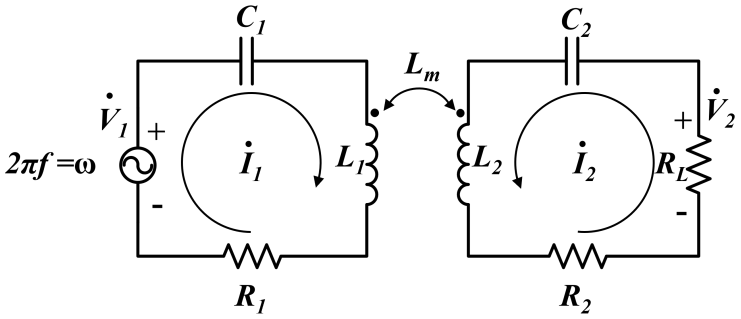

Figure 2. Equivalent circuit of the series-series (SS) WPT via magnetic resonance coupling.

When the coil on the power receiving side is deformed, the self-inductance of the power receiving side L_2, and the mutual inductance between the power transmitting and receiving sides L_m change. This happens because the coil deformation leads to the change of flux linkage in the coil, while self-inductance is the proportional coefficient between the current flowing in the coil and the flux linkage, and the mutual inductance is the proportional coefficient between the current flowing in one coil and the flux linkage in the other coil in a pair of coils.

As for the mutual inductance L_m, the higher L_m value, which means the stronger magnetic field coupling between the coils, leads to the higher transmission efficiency. On the other hand, as for the self-inductance L_2, the combined reactance with the series-

connected capacitor C_2, which is represented as X_r, affects the transmission efficiency as shown in Equation (1). In detail, the maximum value is reached when the receiver side reactance X_r becomes 0.

$$\eta = \frac{R_L(\omega L_m)^2}{R_1\left\{(R_2+R_L)^2+(X_r)^2\right\}+(\omega L_m)^2(R_2+R_L)} \tag{1}$$

where

$$X_r = \omega L_2 - \frac{1}{\omega C_2} \tag{2}$$

From this, it is natural to come up with a method of resonance compensation that maximizes the transmission efficiency by controlling capacitor C_2 against the variation of inductance L_2 caused by changes in the flexible coil's shape and thereby maintains the resonant state (to keep the reactance X_r at 0). This means controlling capacitor C_2 as self-inductance L_2 changes so that Equation (3) is always satisfied.

$$C_2 = \frac{1}{\omega^2 L_2} \tag{3}$$

In this study, we introduce a simple capacity control circuit that can electronically control the equivalent capacitance value of capacitor C_2 and propose an automatic resonance compensation system that maintains the maximum efficiency using this circuit in a fully automatic manner. In the next section, this capacity control circuit and automatic resonance compensation system are detailed.

3. Proposed Automatic Resonance Compensation System

3.1. Overview

The proposed automatic resonance compensation system maintains the resonant state by electronically controlling the equivalent capacitance value of the capacitor against the inductance variation caused by changes in the shape of the flexible coil. This section first details the capacity control circuit that makes the electronic control of equivalent capacitance value possible, and then looks at the resonance compensation algorithm used in case this capacity control circuit is mounted on the receiver side.

3.2. Capacity Control Circuit

3.2.1. Capacity Control Methods

Various methods of electronic control of equivalent capacitance values have been proposed to date, and there are some studies applying these methods to WPT. The first example is an intuitive method that switches the connection of the multiple capacitors arranged in array [19,20]. While easy to implement and control, this method has a limitation that it can only control discrete capacitance values. Then, there is a method that uses voltage controlled capacitors frequently used in the field of communications [21]. While this method realizes continuous capacitance values, the fact that the voltage on the power line itself changes the capacitor value limits its use for low-power transmission.

In contrast to these methods, a method which employ semiconductor switches could realize continuous capacitance values with high power transmission [22–30]. The method that uses zero volt switching (ZVS) to reduce switching loss [22] is superior in terms of transmission efficiency, but it must be used alongside an inverter capable of switching control to synchronize the switching timing. However, though the slight unavoidable switching loss occurs, more convenient capacity control method that can be used independently from the inverter switching control is proposed [23–25]. To emphasize versatility, we chose to design the capacity control circuit based on this convenient capacity control (hereinafter referred to as "conventional capacity control circuit").

Conventional capacity control circuit has only been used in parallel-parallel (PP) WPT via magnetic resonance coupling [23–25]. Previous studies dedicated to the use of WPT in implantable devices have used it as a component of resonance inverter to draw as much power as possible by adjusting the resonance frequency to that maximizes the transmission efficiency. This frequency varies according to changes in the coupling coefficient due to variations in the distance between transmitter and receiver coils, changes in the load impedance according to the state of charge of the energy storage device, and changes in element constants due to electrical coupling between living tissues [23,24]. In another example, a conventional capacity control circuit was used as a high-power source of medical devices. Here, it was used as a component of resonance inverter to prevent resonance loss due to temperature drift, aging, and manufacturing dispersion [25]. In all these cases, a conventional capacity control circuit was used as a resonance capacitor of a transmitter side parallel resonant circuit in PP WPT via magnetic resonance coupling.

In this study, however, it is used as a resonance capacitor of a receiver side series resonant circuit in SS WPT via magnetic resonance coupling. The reason why SS WPT is chosen instead of topology such as SP WPT is because the optimum load value, which shows the maximum transmission efficiency, appears to be closer to the load values of typical mobile devices.

In this case, it is not possible to apply a conventional capacity control circuit as it is.Therefore, the following section explains the detailed structure of a conventional capacity control circuit also describing the current problem of applying it for SS system, as well as an improvement made into a capacity control circuit so that it can be used in SS system.

3.2.2. Details of the Conventional Capacity Control Circuit and Its Problem in Applying for SS System

Figure 3 shows a conventional capacity control circuit. It is composed of a control capacitor C_s, two semiconductor switches placed at both ends of control capacitor C_s, a fixed base capacitor for voltage reference C_r, and a phase controller (Figure 4).

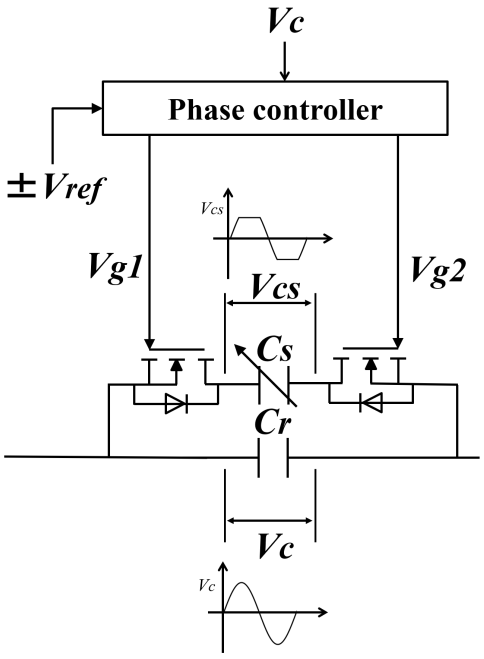

Figure 3. Configuration of the capacity control circuit.

The phase controller compares V_c (terminal voltage of the fixed capacitor C_r) and control voltage $\pm V_{ref}$ and outputs gate signals V_{g1} and V_{g2} (Figure 5).

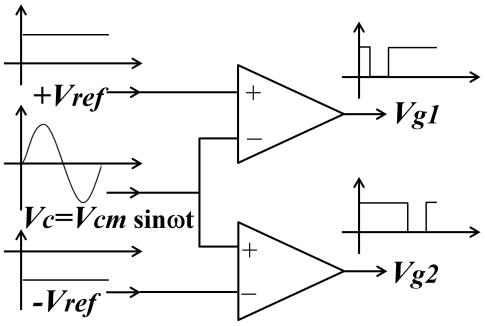

Figure 4. Detail of the phase controller.

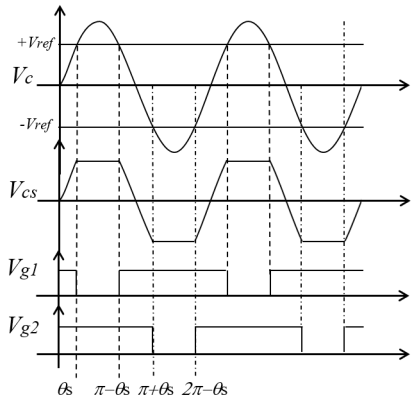

Figure 5. The waveform V_c, V_{cs}, V_{g1}, and V_{g2}.

This gate signal controls the switches at both ends. With this, the conduction and non-conduction of the control capacitor C_s are switched, and therefore, leads to the changes in V_{cs} (the voltage across the control capacitor C_s).

By changing V_{ref}, it is possible to control the duty cycle (the ratio of time the capacitor is conductive), and a continuous change of the equivalent capacitance below the original capacity C_s can be realized. The theoretical value of equivalent capacitance C_{eq} could be expressed as Equation (6), using the phase angle parameter θ_s shown in Equation (4) that describes the switching timing of the switches linked by the duty cycle. Here, V_{cm} is the amplitude value of V_c.

Equation (6) is derived from Equation (5) which represents that the stored charge integrated over a half cycle is equal for the switching-controlled capacitor C_s and the capacitor C_{eq} that shows the equivalent capacitance value. In other words, assuming that a sinusoidal voltage V_c is applied, the capacitor with an effective capacitance value of stored charge equivalent to that of the control capacitor C_s is called the equivalent capacitance C_{eq}.

$$\theta_s = \arcsin\left(\frac{V_{ref}}{V_{cm}}\right) \tag{4}$$

$$\int_0^{\pi} C_{eq} V_{cm} \sin\theta d\theta = \int_0^{\pi} C_s V_{cs} d\theta \tag{5}$$

$$C_{eq} = \frac{2C_s[1-\cos\theta_s] + C_s \sin\theta_s[\pi - 2\theta_s]}{2} \tag{6}$$

The equivalent capacitance value of the entire circuit, C_{total}, is represented by Equation (7):

$$C_{total} = C_r + C_{eq} \quad (7)$$

In case a conventional capacity control circuit is used as a resonance capacitor of a transmitter-side parallel resonant circuit in PP WPT via magnetic resonance coupling, terminal voltage V_c of the fixed capacitor (which is a reference voltage) is constant, and therefore, the duty cycle and control voltage V_{ref} are in one-to-one correspondence. However, when it is used as a resonance capacitor of the receiver side series resonant circuit in an SS system, the reference voltage V_c varies, and therefore, it is necessary to set control voltage V_{ref} according to reference voltage V_c to realize the desired duty cycle. Hence, it becomes important to improve the conventional capacity control circuit so that it can support changes in the reference voltage.

3.2.3. Improved Capacity Control Circuit

Figure 6 shows a capacity control circuit that can support changes in the reference voltage. The circuit is formed by a capacity controller, a generator of control voltage $\pm V_{ref}$, and an extractor of terminal voltage V_c. C_s is a control capacitor that changes the equivalent capacitance value and C_r is a base capacitor with fixed value to obtain terminal voltage V_c.

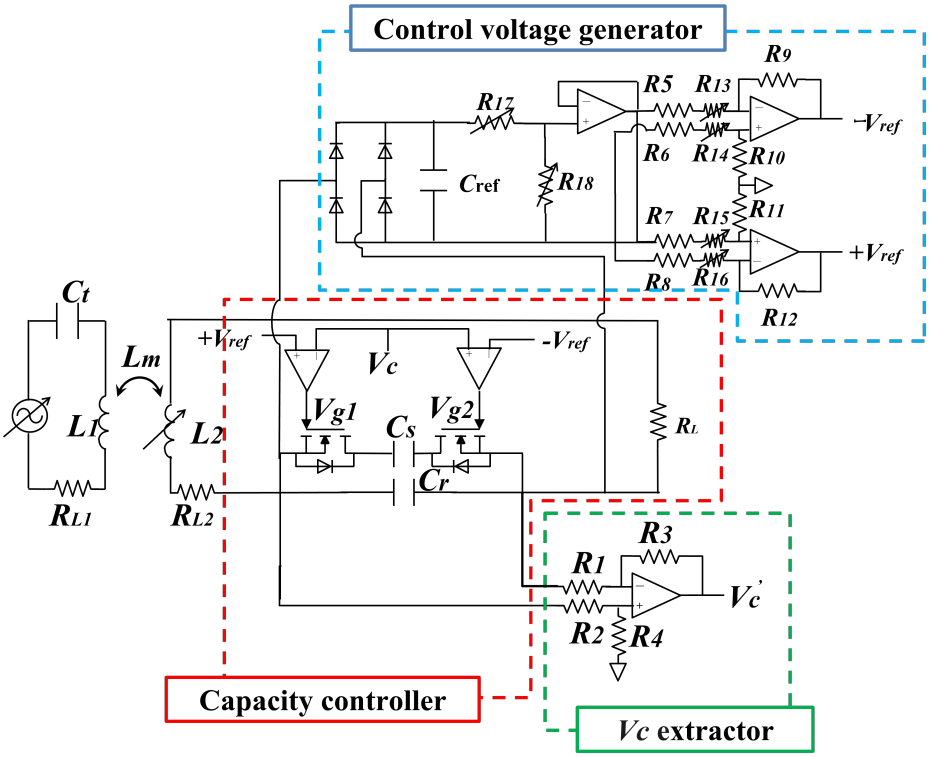

Figure 6. The entire circuit including the modified capacitance control circuit.

The newly added control voltage generator generates control voltage $\pm V_{ref}$ by rectifing terminal voltage V_c, dividing the voltage by a voltage divider circuit, and passing through the differential amplifier circuit. Here, the gain of differential amplifier circuit is controlled by an electronically controllable resistor (digital potentiometer) R_{13}~R_{16}, and the voltage divider circuit with variable resistors R_{17} and R_{18} is inserted to allow the digital potentiometer to be operated in appropriate voltage range.

As the control voltage $\pm V_{ref}$ is generated by multiplying terminal voltage V_c by the differential circuit gain, the duty cycle and differential circuit gain are in one-to-one correspondence regardless of the terminal voltage.

Details on how to determine each resistance value are as follows. First, the relation between V_c and V_{ref} could be described as follows, where we assume that R_5~R_{12} = R_a, R_{13}~R_{16} = R_p holds, and R_p represents the resistance value of digital potentiometer.

$$V_c = V_{cm} sin\omega t \tag{8}$$

$$V_{ref} = \frac{R_a R_{18} V_{cm}}{\sqrt{2}(R_{17} + R_{18})(R_a + R_p)} \tag{9}$$

Then, determining the control range of the digital potentiometer resistance value R_p as follows,

$$R_p^{min} \leq R_p \leq R_p^{max} \tag{10}$$

the control range of the V_{ref} could be expressed as follows.

$$V_{ref}^{min} = \frac{R_a R_{18} V_{cm}}{\sqrt{2}(R_{17}+R_{18})(R_a + R_p^{max})} \leq V_{ref} \leq \frac{R_a R_{18} V_{cm}}{\sqrt{2}(R_{17}+R_{18})(R_a + R_p^{min})} = V_{ref}^{max} \tag{11}$$

Incidentally, the terminal voltage extractor works as an adjustment function to define the duty ratio range by balancing the voltage level between the V_c and V_{ref}. Here, the output voltage of the terminal voltage extractor V'_{cm} works as the actual reference voltage to determine the duty ratio. If we put the amplitude component of V'_c as V'_{cm}, the relationship with V_{cm} becomes as follows, where assuming R_1 = R_2 and R_3 = R_4.

$$V'_{cm} = \frac{R_3}{R_1} V_{cm} \tag{12}$$

Therefore, the duty ratio range could be determined as $D_{min} = \frac{2}{\pi} \arcsin\left(\frac{V_{ref}^{min}}{V'_{cm}}\right) < D \leq 1$ by setting appropriate resistance values for R_1 and R_3 to satisfy $V_{ref}^{min} < V'_{cm} < V_{ref}^{max}$. Thus, the range of the equivalent capacitance C_{eq} could be derived by Equation (6) and following equation which is the relation between the phase angle parameter θ_s and the duty ratio.

$$\theta_s = \frac{\pi}{2} D \tag{13}$$

3.3. Resonance Compensation Algorithm

This section details the fully automatic resonance compensation method that maintains the maximum efficiency using a capacity control circuit.

Here, the following explanation is based on equivalent circuit expressed as Figure 2. Firstly, the relationship between transmission efficiency and receiver side reactance is expressed by Equation (1); the maximum transmission efficiency is reached when the reactance is 0. Therefore, the basic concept of this technique is to control capacitor C_2 with respect to self-inductance L_2 (corresponding to the coil shape) so that it satisfies Equation (3). The capacitor C_2 is controlled by capacity control circuit introduced above.

Since measuring self-inductance L_2 itself is difficult, one of the promising solution is to focus on the fact that the characteristic curve of transmission efficiency η relative to capacitor C_2 is unimodal and use the hill-climbing method to search for the maximum value. However, in order to derive the transmission efficiency, which is calculated as the ratio of the active power transmitted and received, phase difference measurement between voltage and current which is somewhat complex is required since the active power on the transmitter side is determined by multiplying the power factor calculated from the phase difference by the apparent power. Hence, instead of the active power, we decided to use the apparent power, which can be easily derived as the product of the

effective values of voltage and current amplitude. In detail, the ratio of apparent power on the transmitter and receiver sides named as apparent power ratio S_r is introduced and resonance compensation is performed by searching capacitor C_2 that maximizes the apparent power ratio S_r. The measurement system becomes simpler in this approach since it appears not necessary to obtain the phase difference.

For this method to function properly, it is necessary that the characteristic curve of the apparent power ratio S_r relative to capacitor C_2 is unimodal and becomes resonant state at its peak, and therefore, maximizes transmission efficiency η at the same time.

Assuming that the transmitter side is in resonant state, Equation (14) holds according to Kirchhoff's voltage law:

$$\begin{bmatrix} \dot{V}_1 \\ 0 \end{bmatrix} = \begin{bmatrix} R_1 & j\omega L_m \\ j\omega L_m & R_2 + R_L + j(\omega L_2 - \frac{1}{\omega C_2}) \end{bmatrix} \cdot \begin{bmatrix} \dot{I}_1 \\ \dot{I}_2 \end{bmatrix} \tag{14}$$

The currents of transmitter and receiver side and the load voltage of receiver side are expressed as Equations (15)–(17) using input voltage $\dot{V}_1$.

$$\dot{I}_1 = \frac{R_2 + R_L + j(\omega L_2 - \frac{1}{\omega C_2})}{R_1\{R_2 + R_L + j(\omega L_2 - \frac{1}{\omega C_2})\} + (\omega L_m)^2} \dot{V}_1 \tag{15}$$

$$\dot{I}_2 = \frac{-j\omega L_m}{R_1\{R_2 + R_L + j(\omega L_2 - \frac{1}{\omega C_2})\} + (\omega L_m)^2} \dot{V}_1 \tag{16}$$

$$\dot{V}_2 = -\dot{I}_2 R_L = \frac{j\omega L_m R_L}{R_1\{R_2 + R_L + j(\omega L_2 - \frac{1}{\omega C_2})\} + (\omega L_m)^2} \dot{V}_1 \tag{17}$$

Furthermore, the effective value of the input voltage/current and load voltage/current is expressed by Equation (18), and the apparent power of transmitter and receiver side is expressed by Equation (19):

$$V_{in} = |\dot{V}_1|, \quad I_{in} = |\dot{I}_1|, \quad V_{out} = |\dot{V}_2|, \quad I_{out} = |\dot{I}_2| \tag{18}$$

$$S_{in} = V_{in} I_{in}, \quad S_{out} = V_{out} I_{out} \tag{19}$$

Finally, using Equations (15)–(19), the apparent power ratio S_r is expressed as Equation (20). This equation shows that the characteristic curve of apparent power ratio S_r relative to the reactance of the receiver side X_r is unimodal, and its maximum value is reached when the reactance X_r is 0. This agrees with the condition for the maximum transmission efficiency η to be reached. Therefore, it was proved that maximizing the apparent power ratio S_r with the capacity control using the hill-climbing method is valid.

$$\begin{aligned} S_r &= \frac{S_{out}}{S_{in}} \\ &= \frac{R_L(\omega L_m)^2}{|R_1\{R_2 + R_L + jX_r\} + (\omega L_m)^2||R_2 + R_L + jX_r|} \end{aligned} \tag{20}$$

where

$$X_r = \omega L_2 - \frac{1}{\omega C_2} \tag{21}$$

Figure 7 shows the configuration of the automatic resonance compensation system. The effective values of voltage and current were obtained by measurement devices in

both transmitter and receiver side, and then the computer calculates apparent power ratio S_r, and finally adjusts the values of the variable resistors determining the equivalent capacitance using the hill-climbing method.

A detailed flow of the hill-climbing method is shown in Figure 8. Apparent power ratio S_r at the previous time and the current time are compared, and if the efficiency increased, the direction of adjustment of the capacitance value (the varying direction of the variable resistor value) was maintained, and if the efficiency decreased, it was inverted. In addition, when the efficiency oscillated, it was converged to the maximum value by decreasing the amount of capacitance value adjustment.

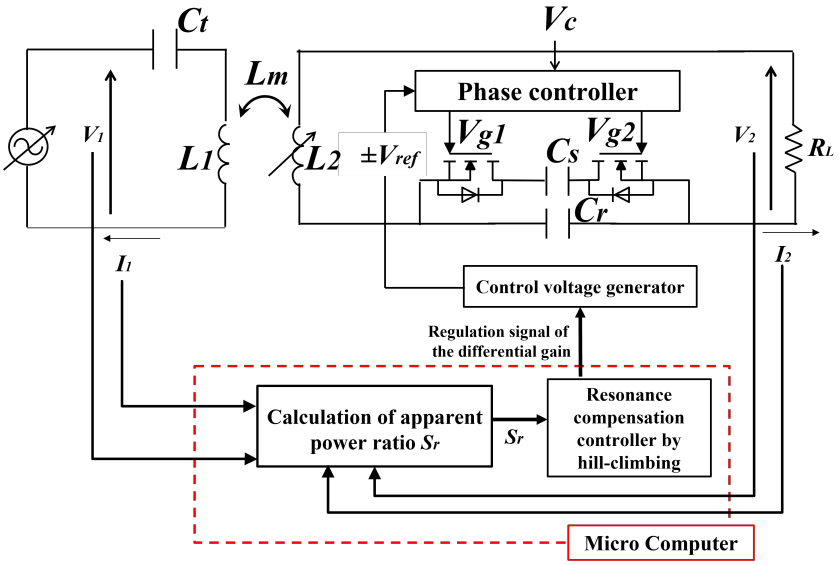

Figure 7. Configuration of the automatic resonance compensation system.

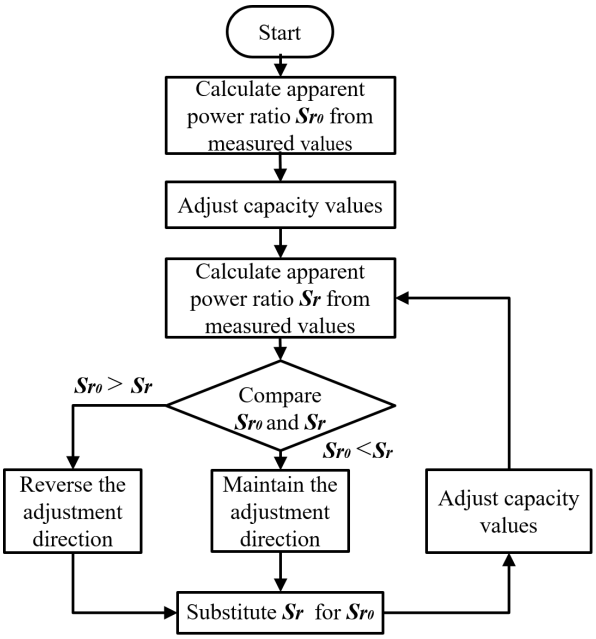

Figure 8. Flowchart of the hill-climbing method.

4. Experiment

4.1. Experimental System

Figures 9 and 10 show the experimental configuration of the automatic resonance compensation system and the experimental environment itself. The power input from

the function generator flows through the power transmitter coil, the power receiver coil, the capacity control circuit, and finally being supplied to the load resistance. The voltage and current of the transmitter and receiver side were measured by an oscilloscope (TBS2104) through a differential voltage probe and a current probe.

The circuit parameters in Figure 6 are shown in Table 1. The flexible deformable coil with a radius of 20 cm and 25 turns were used. A resonance capacitor connected in series to the flexible coil on the power transmitter side is adjusted to realize resonant state at 85 kHz. The capacity control circuit was connected in series to the flexible coil in the receiver side.

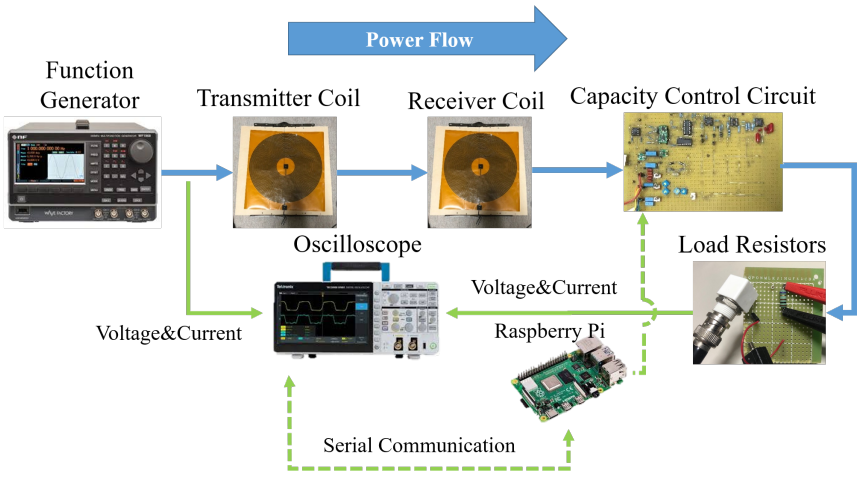

Figure 9. Experimental configuration.

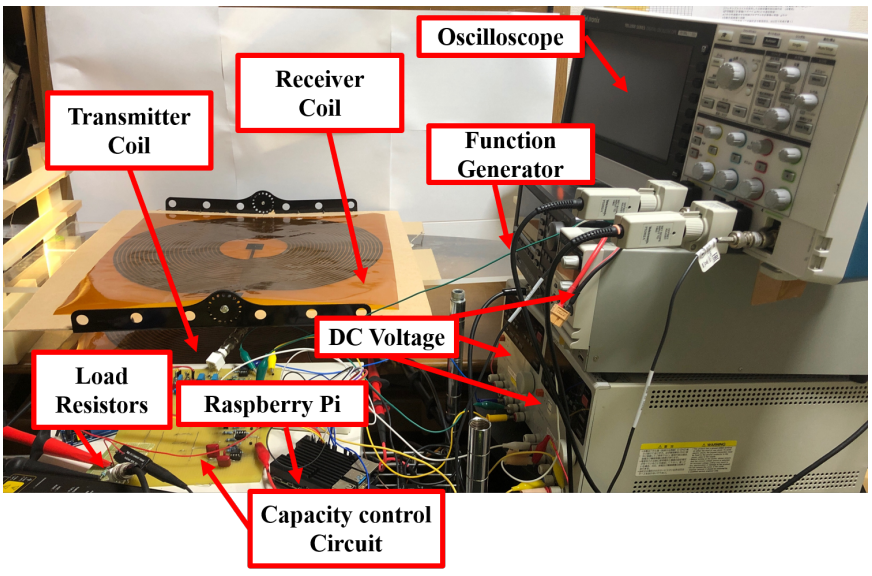

Figure 10. Experimental environment.

The details of the capacity control circuit are as follows. In the control voltage generator, the operational amplifier gain was adjusted by the digital potentiometer used in R_{13}~R_{16}. Moreover, a voltage-dividing resistor was used so that the rated voltage of the digital potentiometer was not exceeded, and to ensure that the division was done correctly, it was insulated by inserting a voltage follower between the partial resistance and the digital potentiometer. To prevent the semiconductor switches from malfunctioning due to a possible voltage shortage in the gate signals of the phase controller, we built a gate driver circuit with a photocoupler (TLP2361). An N-Channel MOSFET (2n7002k) was used as the semiconductor switch of the capacity control circuit.

Table 1. Circuit Parameters.

Symbol	Parameters	Value
f	Frequency	85 kHz
V_{in}	Input Voltage	3.0 V_{pp}
L_1	Inductance of transmitter coil	575.329 μH
L_2	Inductance of receiver coil	573.151 μH
R_{L_1}	Internal resistance of transmitter coil	12.421 Ω
R_{L_2}	Internal resistance of receiver coil	12.4895 Ω
C_t	Capacitor of transmitter side	6094 pF
C_r	Base capacitor of capacity control circuit	4900 pF
C_s	Control capacitor of capacity control circuit	3900 pF
R_1, R_2		1000 kΩ
R_3, R_4		220 kΩ
R_5~R_{12}		7.5 kΩ
R_{13}~R_{16}	Digital potentiometer	0~100 kΩ
R_{17}, R_{18}	Variable resistor	0~200 kΩ
R_L	Load resistance	100 Ω

Raspberry Pi 4 was used as a micro computer. The measured voltage/current of the transmitter and receiver side were input to the computer and the apparent power ratio S_r is calculated. The hill-climbing method is running in the computer and the control value of the digital potentiometer was determined using the apparent power ratio S_r as input. Then, the equivalent capacitance value of the control capacitor C_s was regulated by controlling the digital potentiometer through SPI communication.

Here, it should be noted that the voltage and current of the transmitter should be wirelessly communicated to the receiver in the actual applications. The time delay could be calculated as 1.4 ms per control cycle, assuming transmitted data of 10 bytes (80 bits) and the typical transmission rate of 57,600 bps in Xbee which is common device for wireless communication. Since this delay is small enough compared to the original control cycle of 53 ms, we decided to ignore implementing the wireless communication device in the current system, which focuses in verifying the operation of the proposed efficiency compensation method.

4.2. Efficiency Compensation Relative to the Shape Change of a Flexible Coil

A comparative experiment was carried out to verify the performance of automatic resonance compensation when the shape of a coil changed under three conditions: "Ideal resonance (manually set ideal capacitance value)", "automatic resonance compensation (the proposed method)", and "non-resonant (fixed capacitance value)". The transmission distance between the coils was a horizontal gap of 105 mm.

In terms of the electric circuit model, the purpose of the experiment is to verify the effectiveness of proposed method which automatically controls C_2 to compensate the efficiency by maintaining the resonance when receiver inductance L_2 changes. Therefore, any flexible coil bending pattern which can dynamically change inductance L_2 was acceptable. Thus, as illustrated in Figure 11, the transmission efficiency was measured when the flexible coil on the receiver side was bent from 0 to 120 degrees with an increment of 10 degrees.

First, as the ideal resonance condition, for each bending angle of the flexible coil, the capacitance values of resonance capacitors connected in series were adjusted so that the entire receiver side resonated at 85 kHz. The adjustment was made manually using an impedance analyzer.

Next, as the non-resonant condition, the capacitance value of the resonance capacitors was fixed to a value with which the flexible coil resonated at 85 kHz in a flat condition (with a bending angle of 0 degrees). With this, when the shape of the flexible coil is changed, it appears to be a non-resonant state.

Lastly, as the automatic resonance compensation condition, the automatic resonance compensation using the hill-climbing method mentioned above was applied, and the results were measured at a steady state, after a considerable amount of time.

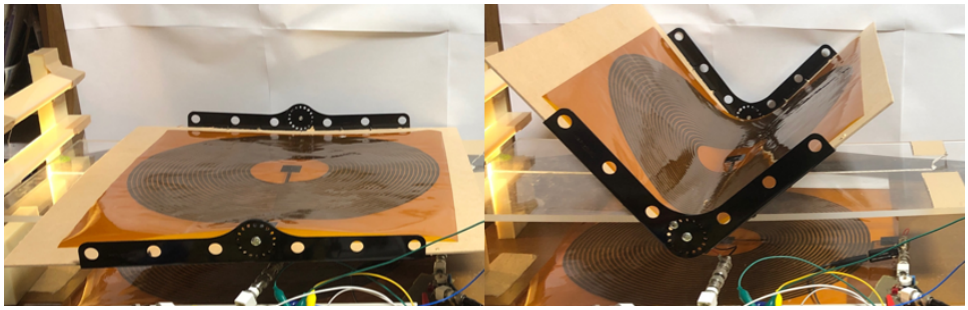

(**a**) (**b**)

Figure 11. (**a**) Bending angle: 0 degrees; (**b**) Bending angle: 90 degrees.

Figure 12 shows how the transmission efficiency changed with respect to the coil bending angle. In the ideal resonance case, the capacitor was adjusted to the coil's bending angle so that it was always at the resonant state, and the transmission efficiency was maximum. In contrast, in the non-resonant case, as the flexible coil's bending angle increased, transmission efficiency η decreased significantly. In the automatic resonance compensation case, the efficiency drop relative to the increasing bending angle was suppressed, and the efficiency varied almost like the case of ideal resonance. When the bending angle was 120 degrees, the transmission efficiency improved by 11.4% compared with the non-resonant case.

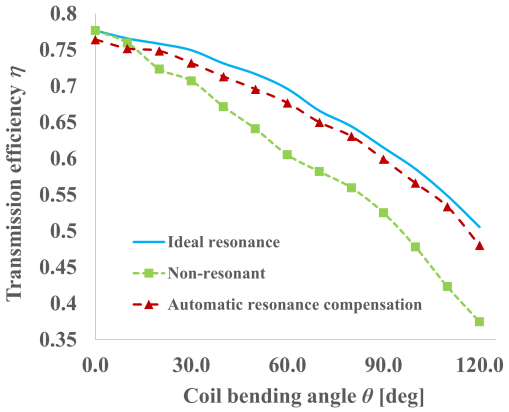

Figure 12. Changes in the transmission efficiency against the coil bending angle under each circuit condition.

However, it should be noted that some part of additional power consumption due to the introduction of the capacitance control circuit were neglected. Therefore, the following is supplementary information on power consumption.

The additional power consumption in detail is considered to be four points: the driving power of the microcontroller, the switching loss, the detection loss in the phase controller, and the driving power of the operational amplifier. Here, the microcomputer (or control unit which works as so) is usually used in the conventional magnetic field resonance WPT system, and therefore, it could be ignored as an increase in power consumption. In addition, the loss of wave detection in the phase controller could be suppressed to negligible level by using a sufficiently large resistance. Therefore, the main part of the additional power consumption is considered to be the switching loss and the driving power of the operational amplifier. Here, the switching loss appears to be proportional to the transmission power, while driving power of the operational amplifier is considered to be

below a certain value. Thus, the experimental results (Figure 12) are derived by accounting only the switching loss as the loss. This means that if the difference of received power in non-resonant case and automatic resonance compensation case is larger than the driving power of the operational amplifier, it is worth implementing the proposed circuit. In the practical case, this could be easily satisfied when the transmitted power is large enough.

Just for reference, the power delivered to the load with respect to the bending angle of the coil for automatic resonance compensation case is shown in Figure 13. It should be noted that since this paper focused on the proposal and basic evaluation of an automatic resonance compensation for WPT using flexible coils, the practicality of the power level was not considered. Therefore, as a future task, we will seek to increase the transmission power for applying the system to real world applications.

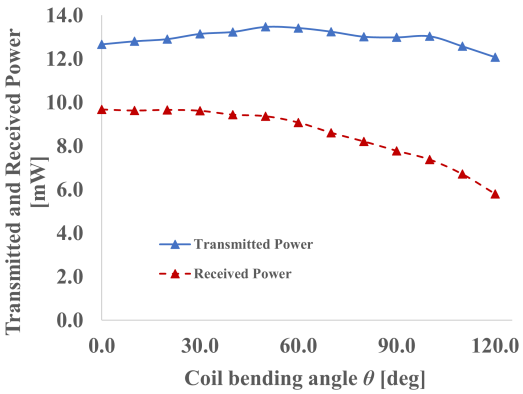

Figure 13. Changes in power delivered to the load against the coil bending angle under automatic resonance compensation condition.

4.3. Responsiveness of the Automatic Resonance Compensation

The next experiment was designed to verify the responsiveness of automatic resonance compensation. First, the capacity control circuit was turned on and put in the resonant state without deforming the flexible coil. Then, the flexible coil was bent 90 degrees while turning off the capacity control circuit (equivalent capacitance value was kept constant in this condition). Due to this, the coil's self-inductance varies, and the resonant state was intentionally lost. Finally, the capacity control circuit was turned on again to observe the transition to the resonant state. We verified the time variation, from the moment the circuit was turned on again until the resonant state was reached, of transmission efficiency η, apparent power ratio S_r, phase difference of voltage and current θ, and total capacitance value C_{total}.

The experiment results are shown in Figures 14 and 15. As time passes, transmission efficiency η improved and the phase difference approached 0, and in response, apparent power ratio S_r and transmission efficiency η gradually approximated. The total equivalent capacitance C_{total} converged in about 1 s and the phase difference θ at the moment of convergence was about 3 degrees, which is 0.9986 if converted to a power factor. Therefore, it could be said that the resonant state has been restored.

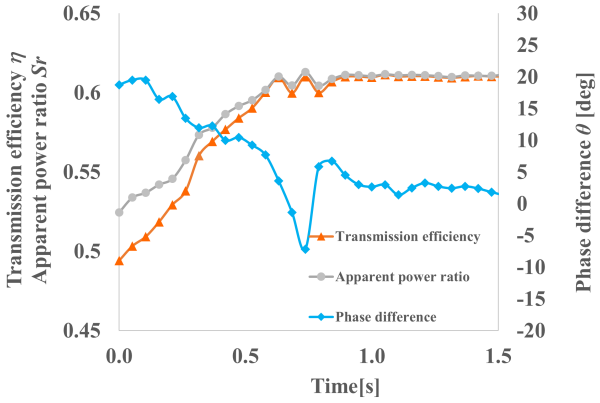

Figure 14. Time variation of apparent power ratio S_r, transmission efficiency η and phase difference.

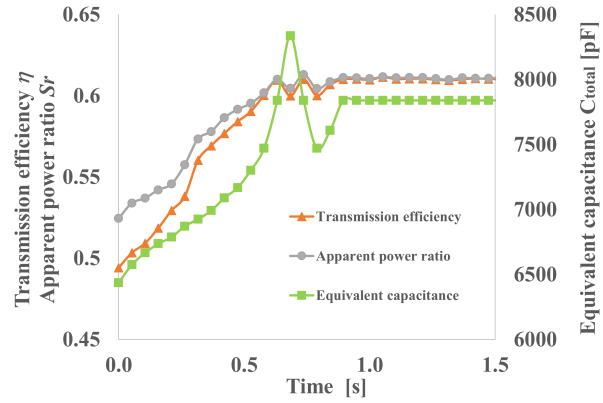

Figure 15. Time variation of apparent power ratio S_r, transmission efficiency η and equivalent capacitance value C_{total}.

5. Conclusions

In this study, we proposed an automatic resonance compensation system for WPT via magnetic resonance coupling using flexible coils, which maintains high transmission efficiency against coil shape changes.

The system works to compensate the collapse of the resonance caused by coil deformation by controlling the equivalent capacitance to maximize the apparent power ratio. To support serial-serial WPT, a feedback circuit was added to the conventional capacity control circuit to control the duty cycle regardless of the reference voltage.

In addition, through actual experiments, we demonstrated that the transmission efficiency was greatly improved compared to the non-resonant state and was maintained at a level comparable to that of ideal resonance, and also that the system showed certain degree of response.

Here, the change in transmission efficiency was measured when the flexible coil was bent in 10-degree increments ranging from 0 to 120 degrees, and succeeded in improving the efficiency by 11.4% compared to the non-resonant state at a bending angle of 120 degrees.

We also confirmed that the time response in restoring the resonant state after the coil was bent at 90 degrees was about 1 s. This means that the current hill-climbing method works fine if the coil shape fluctuates with a cycle of motion sufficiently slower than 1 s, but fails to track it if the fluctuation is much faster than 1 s. Thus, improving the control response might be an future issue in some applications requiring quite high response.

The future works are as follows. First of all, in actual applications, the output voltage from the inverter is not always a sine wave, but often a signal such as square wave. Since the impedance of the circuit depends on the frequency of the signal, the phase difference of the voltage and current is not constant for the fundamental wave and harmonics of

different orders, which are the components of the square wave, and therefore, the apparent power cannot be defined. Therefore, the proposed method of maximizing the apparent power ratio by capacity control using the mountain-climbing method fails in this case. In such a case, maximizing the transmission efficiency directly by the mountain-climbing method might be a good alternative. This should be verified through actual experiments in the future. Moreover, wireless communication should be introduced to send the voltage and current of the transmitter side to the receiver side in the future system. Finally, as an important future task, we will seek to increase the transmission power for applying the system to real world applications.

Author Contributions: Conceptualization, S.N.; methodology, S.N., K.B. and T.M.; data curation, S.N. and K.B.; investigation, S.N. and K.B.; formal analysis, S.N. and K.B.; visualization, K.B.; writing—original draft, S.N., K.B. and T.M.; writing—review and editing, S.N.; supervision, S.N.; project administration, S.N.; funding acquisition, S.N. All authors have read and agreed to the published version of the manuscript.

Funding: This study was supported by the SCOPE (Strategic Information and Communications R & D Promotion Program) No. 205006003 of Ministry of Internal Affairs and Communications and the JSPS KAKENHI 18K04085.

Institutional Review Board Statement: Not applicable.

Informed Consent Statement: Not applicable.

Data Availability Statement: Not applicable.

Conflicts of Interest: The authors declare no conflict of interest.

References

1. Chen, L.; Liu, S.; Zhou, Y.C.; Cui, T.J. An optimizable circuit structure for high-efficiency wireless power transfer. *IEEE Trans. Ind. Electron.* **2013**, *60*, 339–349. [CrossRef]
2. Sample, A.P.; Meyer, D.A.; Smith, J.R. Analysis, experimental results, and range adaptation of magnetically coupled resonators for wireless power transfer. *IEEE Trans. Ind. Electron.* **2011**, *58*, 544–554. [CrossRef]
3. Duong, T.P.; Lee, J.W. Experimental Results of High-Efficiency Resonant Coupling Wireless Power Transfer Using a Variable Coupling Method. *IEEE Microw. Wirel. Compon. Lett.* **2011**, *21*, 442–444. [CrossRef]
4. Kim, J.; Choi, W.S.; Jeong, J. Loop Switching Technique for Wireless Power Transfer Using Magnetic Resonance Coupling. *Prog. Electromagn. Res.* **2013**, *138*, 197–209. [CrossRef]
5. Imura, T.; Hori, Y. Maximizing air gap and efficiency of magnetic resonant coupling for wireless power transfer using equivalent circuit and Neumann formula. *IEEE Trans. Ind. Electron.* **2011**, *58*, 4746–4752. [CrossRef]
6. Kurs, A.; Karalis, A.; Moffatt, R.; Joannopoulos, J.D.; Fisher, P.; Soljac, M. Wireless Power Transfer via Strongly Coupled Magnetic Resonances. *Science* **2007**, *317*, 83–86. [CrossRef]
7. Nakamura, S.; Koma, R.; Hashimoto, H. Efficient Wireless Power Transmission based on Position Sensing using Magnetic Resonance Coupling. *SICE J. Control Meas. Syst. Integr.* **2012**, *5*, 153–161. [CrossRef]
8. Nakamura, S.; Namiki, M.; Sugimoto, Y.; Hashimoto, H. *Q* Controllable Antenna as a Potential Means for Wide-Area Sensing and Communication in Wireless Charging via Coupled Magnetic Resonances. *IEEE Trans. Power Electron.* **2017**, *32*, 218–232. [CrossRef]
9. Jang, Y.; Jovanovic, M.M. A contactless electrical energy transmission system for portable-telephone battery chargers. *IEEE Trans. Ind. Electron.* **2003**, *50*, 520–527. [CrossRef]
10. Farinholt, K.M.; Park, G.; Farrar, C.R. RF Energy Transmission for a Low-Power Wireless Impedance Sensor Node. *IEEE Sens. J.* **2009**, *9*, 793–800. [CrossRef]
11. Kawashima, N.; Takeda, K. Laser energy transmission for a wireless energy supply to robots. *Robot. Autom. Constr.* **2008**, *10*, 373–380.
12. Yang, D.X.; Hu, Z.; Zhao, H.; Hu, H.F.; Sun, Y.Z.; Hou, B.J. Through-Metal-Wall Power Delivery and Data Transmission for Enclosed Sensors: A Review. *Sensors* **2015**, *15*, 31581–31605. [CrossRef] [PubMed]
13. Yamakawa, M.; Mizuno, Y.; Ishida, J.; Komurasaki, K.; Koizumi, H. Wireless power transmission into a space enclosed by metal walls using magnetic resonance coupling. *Wirel. Eng. Technol.* **2014**, *5*, 19–24. [CrossRef]
14. Shimamura, K.; Komurasaki, K. Wireless power transmission into metallic tube using axial slit for infrastructure diagnostics. *Wirel. Eng. Technol.* **2015** *6*, 50–60. [CrossRef]
15. Shimamura, K.; Koizumi, M.; Mizuno, Y.; Komurasaki, K. Effect of Axial Slit on Metallic Tube for Wireless Power Transfer via Magnetic Resonance Coupling: Application of Magnetic-Resonance Coupling Techniques for Infrastructure Diagnostics. *Electr. Eng. Jpn.* **2016**, *197*, 46–54. [CrossRef]

16. Hou, T.; Xu, J.; Elkhuizen, W.S.; Wang, C.C.L.; Jiang, J.; Geraedts, J.M.P.; Song, Y. Design of 3D Wireless Power Transfer System Based on 3D Printed Electronics. *IEEE Access* **2019**, *7*, 94793–94805. [CrossRef]
17. Wen, F.; Jing, F.; Li, Q.; Li, R.; Liu, L.; Chu, X. Curvature Angle Splitting Suppression and Optimization on Nonplanar Coils Used in Wireless Charging System. *IEEE Trans. Power Electron.* **2020**, *35*, 9070–9081. [CrossRef]
18. Imura, T.; Hori, Y. Unified Theory of Electromagnetic Induction and Magnetic Resonant Coupling. *IEEJ Trans. Ind. Appl.* **2015**, *135*, 697–710. [CrossRef]
19. Beh, T.C.; Kato, M.; Imura, T.; Oh, S.; Hori, Y. Automated impedance matching system for robust wireless power transfer via magnetic resonance coupling. *IEEE Trans. Ind. Electron.* **2013**, *60*, 3689–3698. [CrossRef]
20. Lim, Y.; Tang, H.; Lim, S.; Park, J. An adaptive impedance-matching network based on a novel capacitor matrix for wireless power transfer. *IEEE Trans. Power Electron.* **2014** , *60*, 4403–4413. [CrossRef]
21. Porto, R.W.; Brusamarello, V.J.; Pereira, L.A.; Sousa, F.R. Fine tuning of an inductive link through a voltage-controlled capacitance. *IEEE Trans. Power Electron.* **2017**, *32*, 4115–4124. [CrossRef]
22. Zhang, J.; Zhao, J.; Zhang, Y.; Deng, F. A Wireless Power Transfer System with Dual Switch-Controlled Capacitors for Efficiency Optimization. *IEEE Trans. Power Electron.* **2020**, *35*, 6091–6101. [CrossRef]
23. Si, P.; Hu, A.P.; Malpas, S.; Budgett, D. A frequency control method for regulating wireless power to implantable devices. *IEEE Trans. Biomed. Circuits Syst.* **2008**, *2*, 22–29. [CrossRef] [PubMed]
24. Mohamadi, T. Working frequency in wireless power transfer for implantable biomedical sensors. In Proceedings of the 2011 International Conference on Electrical Engineering and Informatics, Bandung, Indonesia, 17–19 July 2011; pp. 1–5.
25. Denieport, R.; Rodes, F.; Zhang, M.; Wang, X.; Ren, X. Medical power generator using a voltage mode resonant converter controlled by a synchronous switched capacitor is MRI compatible. In Proceedings of the 21st IEEE International Conference on Electronics, Circuits and Systems (ICECS), Marseille, France, 7–10 December 2014; pp. 530–533.
26. Rodes, F.; Zhang, M.; Denieport, R.; Wang, X. Optimization of the Power Transfer Through Human Body With an Auto-Tuning System Using a Synchronous Switched Capacitor. *IEEE Trans. Circuits Sysems II* **2015**, *62*, 129–133. [CrossRef]
27. Driscol, S.D.O. A mm-sized implantable power receiver with adaptive matching. In Proceedings of the IEEE Sensors, Waikoloa, HI, USA, 1–4 November 2010; pp. 83–88.
28. Dissanayake, T.; Budgett, D.; Hu, A.P.; Malpas, S.; Bennet, L. Transcutaneous Energy Transfer System for Powering Implantable Biomedical Devices. In Proceedings of the 13th International Conference on Biomedical Engineering, Singapore, 3–6 December 2008; pp. 235–239.
29. Si, P.; Hu, A.; Budgett, D.; Malpas, S.; Yang, J.; Gao, J. Stabilizing the operating frequency of a resonant converter for wireless power transfer to implantable biomedical sensors. In Proceedings of the 1st International Conference on Sensing Technology, New Zealand, 21–23 November 2005; pp. 477–482.
30. Su, Y.G.; Zhang, H.Y.; Wang, Z.H.; Hu, A.P.; Chen, L.; Sun, Y. Steady-State Load Identification Method of Inductive Power Transfer System Based on Switching Capacitors. *IEEE Trans. Power Electron.* **2015**, *30*, 6349–6355. [CrossRef]